Research Article

A new strategy to achieve the controllable preparation of nanoceramics with $BaTiO_3$@resin core–shell nanoparticles

Xiaoting Zhang[1] · Lili Zhao[2] · Bin Cui[1] · Run Zhang[1] · Quan Jin[1] · Jia Wang[1]

Received: 14 May 2020 / Accepted: 28 September 2020 / Published online: 10 October 2020

Abstract
In this paper, phenolic resin (PR) is coated on the monodispersed $BaTiO_3$ nanopowders (C-BTO) prepared by the co-precipitation method via a core–shell manner. This PR can optimize nanopowders' dispersibility in the granulation, and act as a grain growth inhibitor during sintering. So $BaTiO_3$ nanoceramics with dense and size-controlled morphology were achieved at a low sintering temperature. The microstructural and dielectric studies show that the grain size and dielectric properties initially increase and then decrease as the amount of PR increases. Moreover, the activation of PR is optimal at 20 wt%, and obtained ceramics have a high density and uniform grain size, with a relatively high dielectric constant (ε_{max}) of 3545 and low dielectric loss (tanδ) of 0.011. Besides, by tailoring the particle size of C-BTO@PR powders, dense $BaTiO_3$ ceramics with mean size of 135–308 nm can be obtained with sizes similar to initial particle. The results demonstrate that PR coated $BaTiO_3$ nanopowders in core–shell structure is an effective strategy to prepare $BaTiO_3$ nanoceramics controllably.

Keywords Phenolic resin · Core–shell · Dispersibility · Nanoceramics

1 Introduction

Toward the miniaturization and integration for producing ceramic devices, nanoceramics have become urgently needed in multilayer ceramic capacitors. Moreover, excellent dielectric breakdown strength and delayed polarization saturation make them promising candidates for high-energy storage devices [1]. Nanoceramics not only refer to a class of ceramics whose grains and grain boundaries are at the nanometer level (1–100 nm), but more deeply refer to the grain threshold that causes sudden changes in their phase structure or performance [2]. However, the critical size at which the size effect occurs differs due to the variety of synthesis routes and processing techniques adopted. For example, the critical size reported in the literature for the transition from the ferroelectric to cubic paraelectric phase ranges from a few nanometers to tens of nanometers [3–5]. $BaTiO_3$ nanoceramics, which have unique high reliability and capacitance volumetric efficiency, are particularly outstanding [6]. Whereas, it is extremely difficult to obtain dense nanoceramics with nanometer sizes (< 100 nm), due to the ease of grain growth of nanoparticles. Up to now, several fabrication techniques about $BaTiO_3$ nanoceramics have been explored. One is about the controllable synthesis of $BaTiO_3$ nanopowders. $BaTiO_3$ powders prepared by solid phase method commonly have large grain size (> 1 μm) and inhomogeneous particle size distribution, making them unsuitable for high performance ceramics [7]. An alternative choice is chemical methods like co-precipitation, which was utilized to prepare powders with good dispersibility and controllable particle size, thereby facilitating the controllable

✉ Bin Cui, cuibin@nwu.edu.cn | [1]Key Laboratory of Synthetic and Natural Functional Molecule Chemistry of Ministry of Education, Shaanxi Key Laboratory of Physico-Inorganic Chemistry, College of Chemistry & Materials Science, Northwest University, Xi'an 710127, Shaanxi, China. [2]School of Information Science and Technology, Northwest University, Xi'an 710127, Shaanxi, China.

preparation of nanoceramics. However, it is difficult to accurately control the stoichiometric ratio in complex compositions due to the loss of some ions during washing [8, 9]. Another extensive research is based on sintering technologies. The conventional sintering is simple but lack of suppression of grain growth. Comparatively speaking, rapid sintering techniques such as microwave sintering and SPS sintering ensure control over grain growth and final microstructure via a rapid rise to high temperature and hold for a short time. Hot-press sintering and two-step sintering enable ceramics highly dense [10–12], but the severe sintering conditions of those techniques make them require either costly equipment or initial nanopowders less than 10 nm. Besides, the addition of glass, such as ZnO-B_2O_3, Li_2O-SiO_2 and BaO-B_2O_3-SiO_2, can sometimes act as a grain growth inhibitor, but their electrical performance was easily weakened due to the heterogeneous impurities [13–15]. So, there are still some problems with the precise synthesis of nanoceramics, including poor controllability or repeatability, high requirements for powder size and dispersion, harsh sintering conditions and the introduction of impurities to degrade performance.

In traditional granulation, ceramic powders were directly mixed with dispersant to a similar pseudo-particle size level for high density, uniformity and mechanical strength. Particularly for the nanopowders with strong agglomeration, the granulation uniformity of dispersant is too poor to obtain nanoceramics. Thus, temporary dispersants play a role in improving ceramics' quality and properties. Great dispersants should meet the following requirements: good wetting and adsorption by ceramic powders, strong adhesion to ensure the strength, and as little residual ash [16]. Nowadays, organic dispersants such as polyvinyl alcohol (PVA), paraffin and phenolic resin (PR) have been widely used in electronic ceramics industry [17]. Among them, pressed with water-based dispersants like PVA, the green body has higher mechanical strength but need to be stored to prevent water evaporation [18–20]. Inversely, oily-based dispersants such as paraffin are non-volatile, but are difficult to remove at high temperatures due to their oxidation [21]. Most notably, owing to its low cost, high bonding strength and adhesion, resin-based dispersants have received extensive attention. For instance, by adding PR and polycarbosilane, Bougoin et al. obtained B_4C ceramic with high relative density of 92% under pressureless sintering [22]. More intriguingly, Schwetz et al. found that the pyrolyzed carbon of PR acts as an inhibitor of surface-surface transport, so as to enhance the densification through grain boundary or lattice diffusion at a lower T_s [23]. Accordingly, PR has been used as a sintering aid to promote densification in the industrial production of B_4C ceramics [24].

As for the mixing way of dispersant, it is directly mixed into ceramic nanopowders in traditional granulation. But it is difficult to achieve uniform distribution of dispersant around ceramics particles, which inevitably cause local pores after sintering. Even if a dispersant is added by ball milling, the molecular chain will be broken to affect its adhesive properties. To deliver a uniform mixing performance, the modification engineering of micro/nanomaterials via core–shell nano-scale mixing technique has been extensively applied to many fields like electronic ceramics and drug carriers. Li et al. found that the core–shell structure of Fe_3O_4@SiO_2 composites should be responsible for their good dispersibility and alleviated agglomeration [25]. Moreover, this special structure could improve the distribution uniformity of glass shell and restrict grain growth, thus achieving the high energy storage performance (10 J cm^{-3}) in $BaTiO_3$/glass core–shell nanoceramics [26]. Similarly, our group has also accumulated rich experience on the controllable preparation of core–shell structured submicron ceramics [27, 28]. Core–shell structure has proven to be an effective method to suppress the grain growth of nanopowders to prepare nanoceramics. Meantime, the core–shell method ensures homogeneous mixing of dispersant and ceramic powders, so it may also act as a dispersant to alleviate the agglomeration.

Since nanopowders have high surface activity and prone to agglomerate, foreseeable phenomena including uneven granulation, uncontrolled grain growth, and poor densification will inevitably occur after sintering. So, it is still extremely challenging to obtain dense nanoceramics with the control of their grain size. Herein, as illustrated in Fig. 1, we use co-precipitation method to prepare well-dispersed $BaTiO_3$ powders, and then the resin-based dispersant PR was coated on them surface to construct a core–shell structure. This way not only makes the C-BTO powders larger to adjust their sintering activity to a similar extent, but also ensure the overall uniformity in green sheets after the molding process. Hereafter, in the initial sintering stage, as a suitable temperature is provided, the tremendous gas mobile phase pyrolyzed from PR pushes nanopowders rearrange and self-assemble to a more compact state. And in the final sintering stage, as a continual increase in temperature, ceramic particles were rearranged secondly via grain boundary migration but simultaneously the residual carbon ash prevents excessive grain growth, so nanoceramics can be obtained at a lower T_s. The effects of PR amount and initial powder size on the morphology, phase composition and dielectric properties of $BaTiO_3$ ceramics were studied. So this work is expected to achieve the controllable preparation of $BaTiO_3$ nanoceramics via the design of core–shell architecture formed by PR coated $BaTiO_3$ nanopowders.

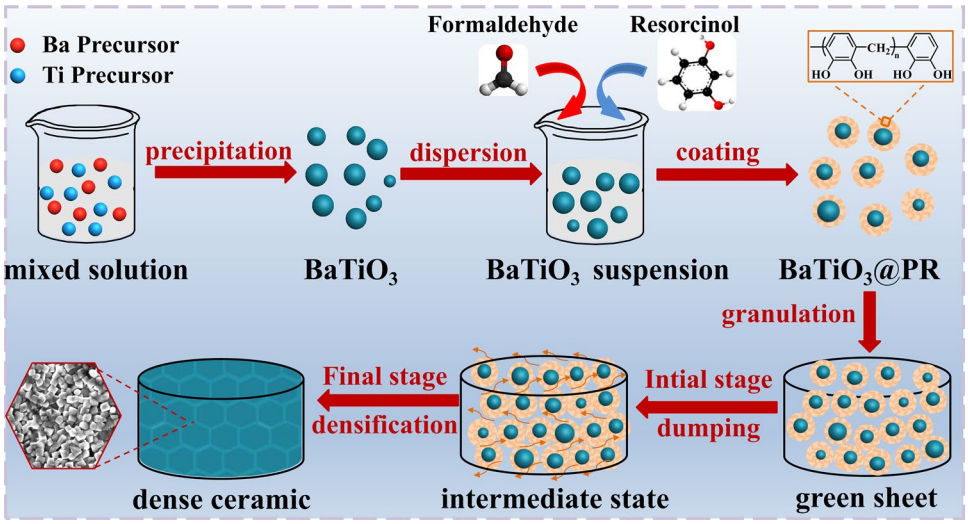

Fig. 1 Preparation process of dense $BaTiO_3$ nanoceramics

2 Materials and methods

2.1 Experimental reagents

Raw materials including titanium tetrachloride ($TiCl_4$, 99.0%), barium acetate ($Ba(CH_3COO)_2$, 99.9%), sodium hydroxide (NaOH, 99.0%), ammonia ($NH_3{\cdot}H_2O$, 25.0 wt%), formaldehyde (HCHO, 37.0–40.0 wt%), resorcinol ($C_6H_6O_2$, ≥ 99.5 wt%) and absolute ethanol (CH_3CH_2OH, 99.7%) are all analytical grade reagents.

2.2 Preparation of $BaTiO_3$@PR powders and $BaTiO_3$ ceramics

Based on our previous work, monodispersed cubic $BaTiO_3$ powder with an average particle size of 178 nm were synthesised using a co-precipitation method [29]. The typical preparation procedures of $BaTiO_3$@PR powders with 20 wt% PR were carried out as follows. $BaTiO_3$ per 1.0 g is sonicated in a mixture containing 80 mL of deionised water, 0.4 mL of aqueous ammonia and 35 mL of absolute ethanol for 1 h to produce a uniform suspension. Then, the resorcinol with content of 0.2 g were added to the above solution. After the mixture was mechanically stirred at 70 °C for 30 min, formaldehyde solution (2:1 molar ratio to resorcinol) was added for polymerization for 24 h. Then, the mixture was centrifuged and dried overnight at 50 °C to obtain $BaTiO_3$@PR powder [30]. Similarly, this method can prepare $BaTiO_3$@PR powders with designed mass fractions of PR ranging from 0, 10, 20, 30 to 40 wt% by controlling the resorcinol contents. Finally, this series of powders were compressed under a pressure of 6 MPa by means of uniaxial pressing, and sintered in the air for 2 h at 1100 °C to obtain ceramics.

To investigate the general applicability of PR dispersant on $BaTiO_3$ ceramics with different initial particle size, a series of prepared $BaTiO_3$ core powders with various size are abbreviated as C-BTO_x ($x = 1, 2, 3$), as the concentration of the NaOH precipitant are 15, 10, 6 mol/L, respectively. The C-BTO_x@PR powders were then prepared with fixed PR mass fraction of 20 wt%. Next, the powders obtained were pressed into pellets under a pressure of 6 MPa and sintered for 2 h at their optimal sintering temperature. Based on the requirements for dense and fine-grained ceramics with grain sizes comparable to initial powders, the optimal sintering temperatures of C-BTO_1, C-BTO_2, C-BTO_3 ceramics were chosen at 940 °C, 980 °C and 1060 °C, respectively.

2.3 Characterization

The phase structure of all powders and ceramics was determined by an X-ray powder diffractometer (XRD, D8 Advance, Bruker, Germany). The surface and internal microscopic morphology of samples were observed using a scanning electron microscope (SEM, Quanta-600, FEI, USA) and transmission electron microscopy (TEM, Tecnai G2F20S-TWIN, FEI, USA), respectively. The size distribution histogram inserted in the SEM was calculated by the Nano Measurer 1.2 software, and the total number of particles counted in each sample was 300. Thermogravimetric (TG) and differential scanning calorimetry (DSC) analysis were performed using a TG/DSC instrument (STA 449 F3, Netzsch, Selb, Germany) at a heating rate of 10 ℃ min^{-1} under an air flow. For electrical performance testing, ceramic samples were coated with silver paste, fired at 550 °C for 0.5 h and characterized using an impedance analyzer (Model HP4284A, Hewlett-Packard, USA) accompanied by a high and low temperature controller measured at 1 kHz.

3 Results and discussion

3.1 Effect of coating amount of PR dispersant on morphology and dielectric properties of $BaTiO_3$ ceramics

Figure 2 shows the morphology and phase composition of C-BTO@PR powders with various amount of PR. It can be seen that as the amount of PR is 0, 10, 20, 30 and 40 wt%, the statistical particle sizes are 178 ± 21, 194 ± 16, 218 ± 11, 234 ± 17 and 253 ± 12 nm, respectively. The partially enlarged TEM Figures are also displayed in the insert of Fig. 2a-e, the thickness extracted from which are 8, 20, 28 and 37 nm, respectively. So the thickness of PR shell gradually increases with the increase of resorcinol concentration. Furthermore, samples coated PR have comparatively smoother surface than pure C-BTO powders, and the PR coating can be easily distinguished. The granulating agent PR is more uniformly distributed and has better dispersibility on the surface of C-BTO powders. This highlights the advantages of the liquid phase in-situ coating method of the granulating agent on the surface of ceramic powders. Specifically, the surface of each ceramic powder is coated with quantitative amount of PR, which overcomes the agglomeration of C-BTO powders and makes them better dispersibility. Whereas, it is impossible to achieve in the traditional granulation of directly mixing between ceramic powders and the granulating agent. Therefore, due to the better uniformity and dispersion of the samples coated with PR, we can assume that PR plays a similar role like surfactants. The XRD patterns of above powders are displayed in Fig. 2f. The major diffraction peaks of perovskite phase for pure C-BTO are strong and sharp. Whereas, the intensity of the major phase decreases with increasing the amount of PR additive due to the typical amorphous feature of PR [31]. Therefore, it proves to be an effective way to avoid the uneven distribution of dispersant in traditional granulation by introducing PR dispersant via a core–shell structure.

TG-DSC measurement is conducted to investigate the thermal behaviour of the C-BTO@PR powders with 20 wt% PR. As shown in Fig. 3, when heated from 20 to 1100 °C, the weight of C-BTO@PR powders gradually decreased and

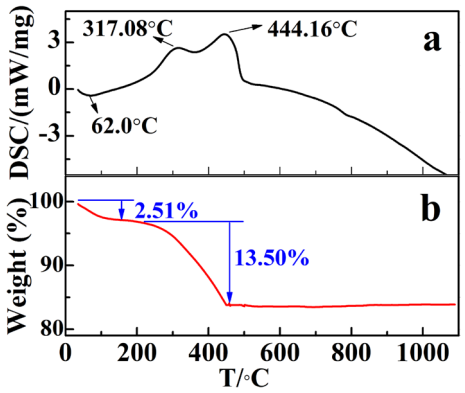

Fig. 3 DSC **a** and TG **b** measurement of C-BTO@PR powder with 20 wt% PR at a heating rate of 10 °C min^{-1} under air flow

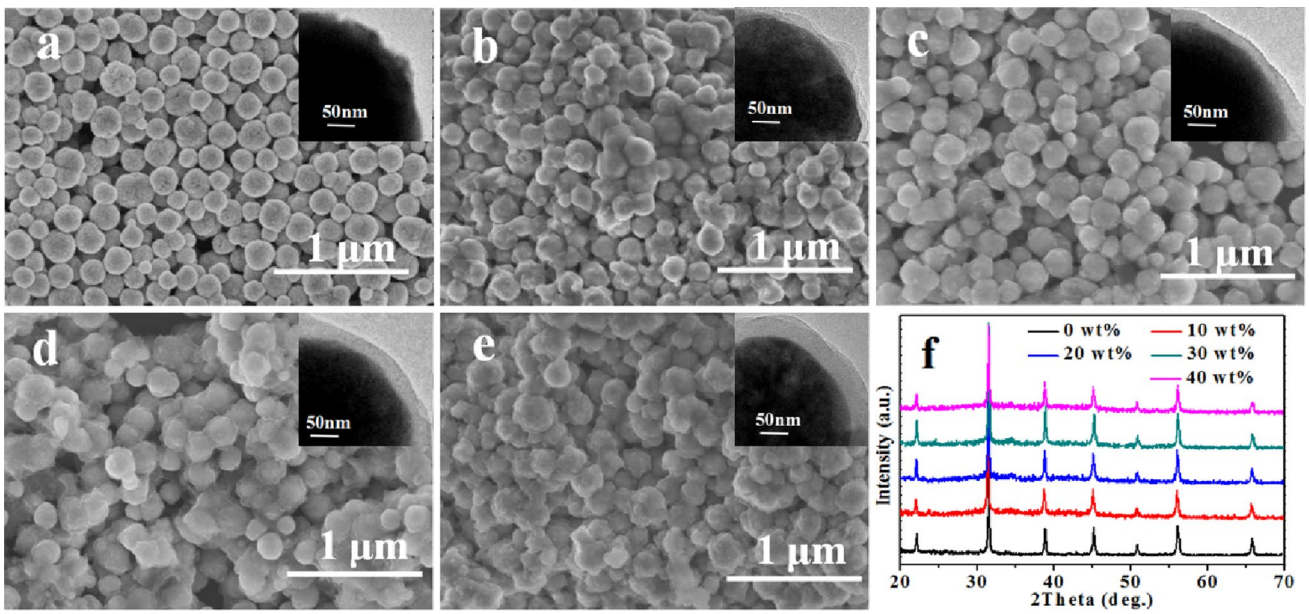

Fig. 2 SEM images, TEM insert images and XRD patterns of C-BTO@PR powders with various amount of PR: **a** 0 wt%, **b** 10 wt%, **c** 20 wt%, **d** 30 wt%, **e** 40 wt%, **f** XRD patterns of all powders

then tended to be horizontal, the total weight loss was 19.11 wt%. To be specific, there are two stages of obvious weight loss. In the initial stage below 198 °C, as the temperature rises, the resin cross-links and solidifies through further condensation [32], and the endothermic polycondensation reaction results in a significant endothermic peak at 62.0 °C. It is mainly a nucleophilic addition reaction between phenol and formaldehyde, and followed by continuous polycondensation reaction, accompanied by solvents and small molecules evaporated such as H_2O and NH_3, so there is less mass loss at this stage (about 2.51%). In the higher temperature range of 198–525 °C, the cross-linked C-O bond and C–C bond of PR are cracked by oxygen attack, and the formed carbon is oxidized. And due to the massive decomposition of the cured PR chains, a large amount of small molecular gases such as CH_4, H_2, CO_2 and H_2O are released. So, this stage suffers from a significant weight loss by 16.60%, which is also confirmed by the strong exothermic peaks at 317.08 °C and 417.16 °C. Therefore, at this stage, the rapid pyrolysis of PR plays a driving role in the ceramic powders to make the rearrangement more compact and effective. In the final stage above 525 °C, the weight of material remains almost constant, which left few residual carbon ash about 3.99 wt% after PR pyrolysis, and the residual formed a barrier layer at the grain boundary so as to suppress the grain growth. It is worth noting that as the PR coating contains a solvent, the initial temperature of the weight loss there is lower than the initial temperature in the literature [33]. The weight loss percentage is greater due to the volatilization of the solvent. In addition, the C-BTO powders prepared by the co-precipitation method have a high energy surface, so it can be used as a nucleation agent to promote the growth and polymerization of PR on its surface, and the polar groups in the PR can be well bonded to it [34]. In summary, the test results further verified that PR was uniformly coated on the BT surface with an amount of 20 wt%.

The SEM images and XRD patterns of ceramics with various amounts of PR dispersant sintered at 1100 °C are presented in Fig. 4. It can be obtained that as the amount of PR dispersant is 0, 10, 20, 30 and 40 wt%, the grain sizes are 192 ± 19, 362 ± 32, 960 ± 54, 408 ± 22 and 301 ± 34 nm. Meanwhile, their values of the relative density are 0.74, 0.92, 0.97, 0.90 and 0.81, respectively, demonstrating that the bulk density initially increased but decreased finally with increasing PR content. Notably, compared with traditional micron-sized $BaTiO_3$ ceramics sintered above 1300 °C in the literature [35], T_s is reduced to 1100 °C, thereby decreasing the production cost. So, the PR coating has proven to effectively promote the sintering activity. As Fig. 4b shows, the denser microstructure appeared in samples with 20 wt% PR, but it exhibited appreciable grain growth because of its high sintering temperature. When the amount of PR exceeds 20 wt%, the increased porosity and aggregates can be ascribed to the generation of large-amount gas phase [36]. To be more specific, the introduction of PR dispersant in a coating manner can activate their surface, thereby reducing the agglomeration of nanopowders and optimizing the non-uniformity distribution in traditional granulation [37]. Figure 4f reveals the XRD patterns of this series of samples, it is noted that the splitting of the 200/002 peak is gradually evident and

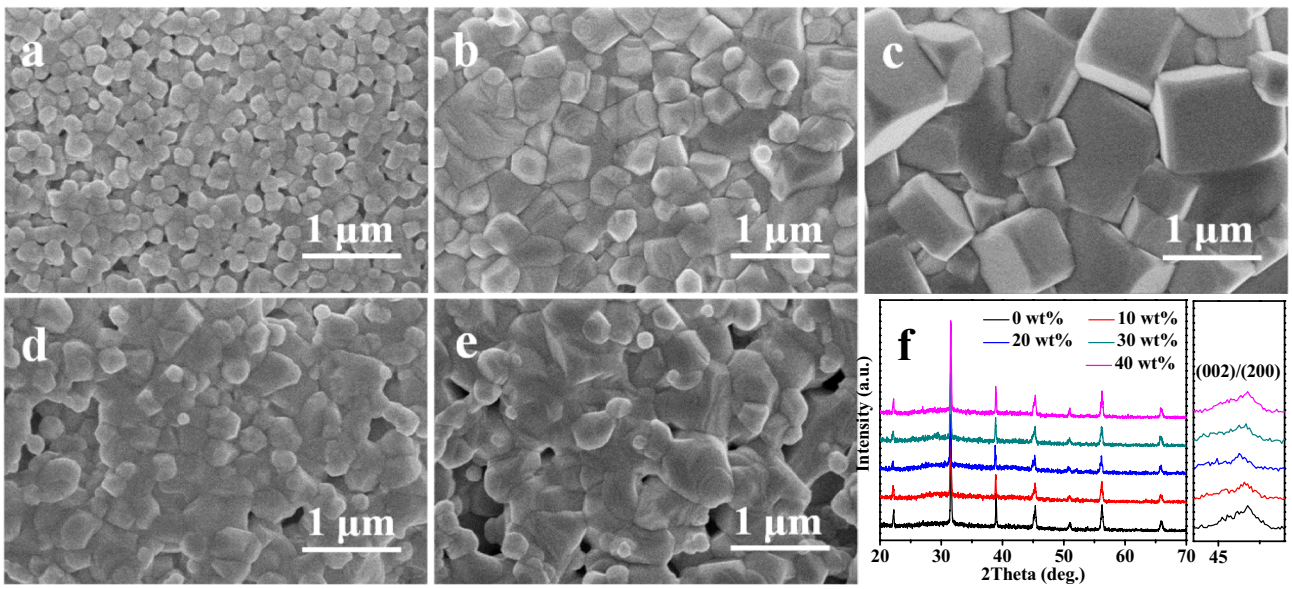

Fig. 4 SEM image and XRD patterns of C-BTO ceramics with various amount of PR sintered for 2 h at 1100 °C. **a** 0 wt%, **b** 10 wt%, **c** 20 wt%, **d** 30 wt%, **e** 40 wt%, **f** XRD patterns of all samples

is most pronounced at 20 wt%, which proves that the sample has the strongest tetragonality. The diffraction peaks slightly moved to a low angle up to 20 wt%, illustrating the gradual expansion of the volume in unit cell which corresponds to the grain size. Therefore, the PR coating effectively optimize nanopowders' dispersibility and promote the sintering activity, and it is particularly noticeable at 20 wt%.

To study the influence of PR dispersant on dielectric properties of $BaTiO_3$ ceramics, Fig. 5 displays the temperature dependence of dielectric permittivity and dielectric loss of samples with various amount of PR. It can be obtained that as the amount of PR is 0, 10, 20, 30 and 40 wt%, the maximum dielectric constant (ε_{max}) is 1974, 2915, 3545, 2486 and 2278, and the tanδ at room temperature is 0.029, 0.024, 0.011, 0.013 and 0.020, respectively. It can be analyzed that due to the role of PR in activating the sintering behavior, the obtained dense $BaTiO_3$ ceramics optimize their dielectric performance. Meanwhile, the ε_{max} and ε_r first increase and then decrease, as the amount of PR increases, which is mainly related to the change of compactness and powder particle size caused by the difference in activation sintering behavior of PR and the content of tetragonal phase. The higher dielectric properties ($\varepsilon_{max} \sim 3545$, tan$\delta \sim 0.011$) of ceramics prepared when the PR content in the BTO@PR powder is 20 wt% should be ascribed to its larger density and coarse-grain size. Further speaking, small amount of PR will prevent the grain growth, while too much amount PR will generate more gas due to its decomposition and the reduction of the ceramic density, so only a proper amount of PR can trigger the maximum activation sintering. Therefore, the PR coating can promote the sintering activity, optimize the sintering densification, and significantly improve its dielectric properties.

3.2 Effect of initial particle size on morphology and dielectric properties of $BaTiO_3$ ceramics

In the above-mentioned study on the coating amount of PR, we determined the role of PR as a sintering activity promoter. As known, the macroscopic properties are greatly influenced by the grain size of ceramics. So, PR and appropriate T_s will be jointly controlled to prepare ceramics with grain size down to nanoscale. The research on the grain size engineering of ceramic materials is conducive to the miniaturization of ceramic capacitors. Figure 6 exhibits the XRD patterns of C-BTO and C-BTO@PR powders. From their typical diffraction analysis, it can be known that as-prepared C-BTO and C-BTO@PR powders all exhibit the cubic perovskite phase with high crystallinity, and no other crystalline impurities were detected. Whereas, due

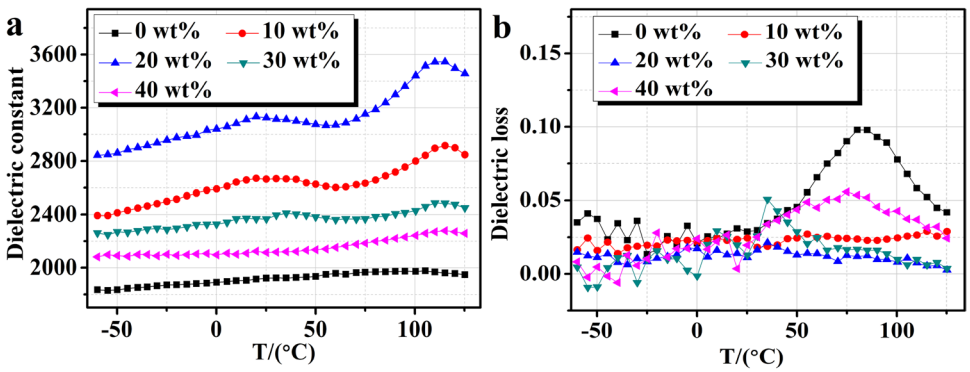

Fig. 5 Temperature dependence of **a** dielectric permittivity and **b** dielectric loss of C-BTO ceramics with various amount of PR

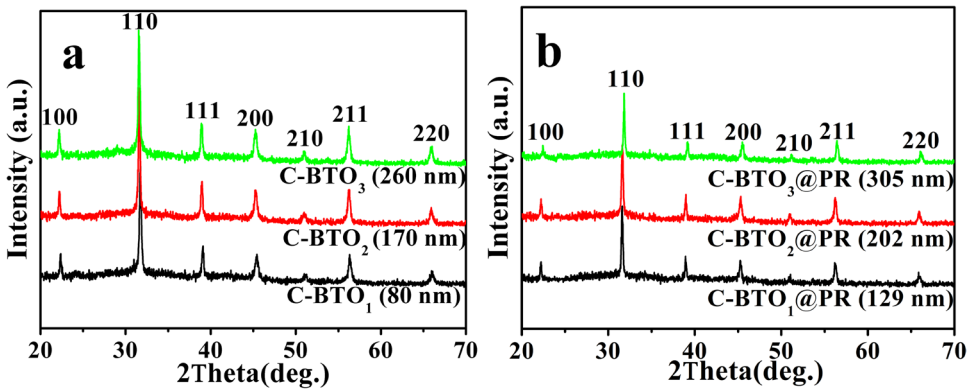

Fig. 6 XRD patterns of **a** C-BTO_x and **b** C-BTO_x@PR powders ($x = 1, 2, 3$) with different particle sizes (The coating content of PR is 20 wt%.)

to the coating of the amorphous PR dispersant, the intensity of each diffraction peak in C-BTO$_x$@PR powders was slightly weaker than that in C-BTO$_x$ ones.

Figure 7 represents SEM images of C-BTO$_x$ and C-BTO$_x$@PR powders with different particle sizes (The coating content of PR is 20 wt%.). It could be statistically concluded as the concentrations of the NaOH precipitant is 15, 10 and 6 mol/L, the particle sizes of C-BTO$_x$ powders are 88 ± 28, 170 ± 23 and 260 ± 19 nm, and the corresponding C-BTO$_x$@PR ones are 129 ± 10, 202 ± 11 and 305 ± 13 nm, respectively. Generally, as the concentration of the precipitant increases, more nucleation centers appear, making it more prone to nucleation than growth, so that smaller powders can be obtained [38]. Furthermore, powders coated with PR exhibit uniform shape with good dispersibility, demonstrating the obvious optimization in microtopography by introducing PR forming a core–shell structure. That is, PR can activate the surface of C-BTO$_x$ powders from rough to smooth, making them grow larger and more uniform to weaken nanopowders' agglomeration. This way can ensure the granulation uniformity of nanopowders, so that it can be rearranged and self-assembled into a compact state during the sintering process, thereby suppressing the abnormal growth of partial grain to prepare nanoceramics [39]. This will lay an experimental basis for the controllable preparation of dense nanoceramics.

Figure 8 depicts the SEM images and XRD patterns of C-BTO$_x$ ceramics at 20 wt% PR with their grain size distribution inserted. It can be obtained that all samples achieve low porosity and consistently high relative densities larger than 95%. Their mean grain sizes are 135 ± 22, 213 ± 15 and 308 ± 10 nm for x = 1, 2 and 3, respectively. Since the coating amount of PR is fixed and the PR is almost completely pyrolyzed after sintering, the effect of PR during sintering is negligible like common PVA, and the influence of the particle size of the core is studied here. Besides, in the early stage of sintering, the distance between the spherical powders is continuously reduced, forming the sintering neck at the contact point of powders. The contact surface of spherical powder is so small that it is not conducive to mass transfer and densification. However, in polycrystalline ceramics, the relative higher heat treatment temperature contributes to the mutual mass transfer of crystal powder, which results in a better crystallization degree of ceramics than powders, so irregular polyhedral morphologies are usually formed in polycrystalline ceramics to form dense ceramic materials, which can be seen from the SEM surface images. Compared with the initial C-BTOx@PR powder, no obvious grain growth was observed in all ceramic samples, which is due to the proper control of the coarsening degree of its size at the respective optimal sintering temperature until the density reaches a similar degree. As we all know, the grain size of ceramics is determined by the starting powder size and sintering conditions. The coating resin will prevent the growth of grains during the sintering process, thereby facilitating the maintenance of initial particle size. Therefore, the grain size of the final ceramics mainly depends on the initial particle size. The purpose of our research is to accurately control the grain size of ceramics through the particle size of initial

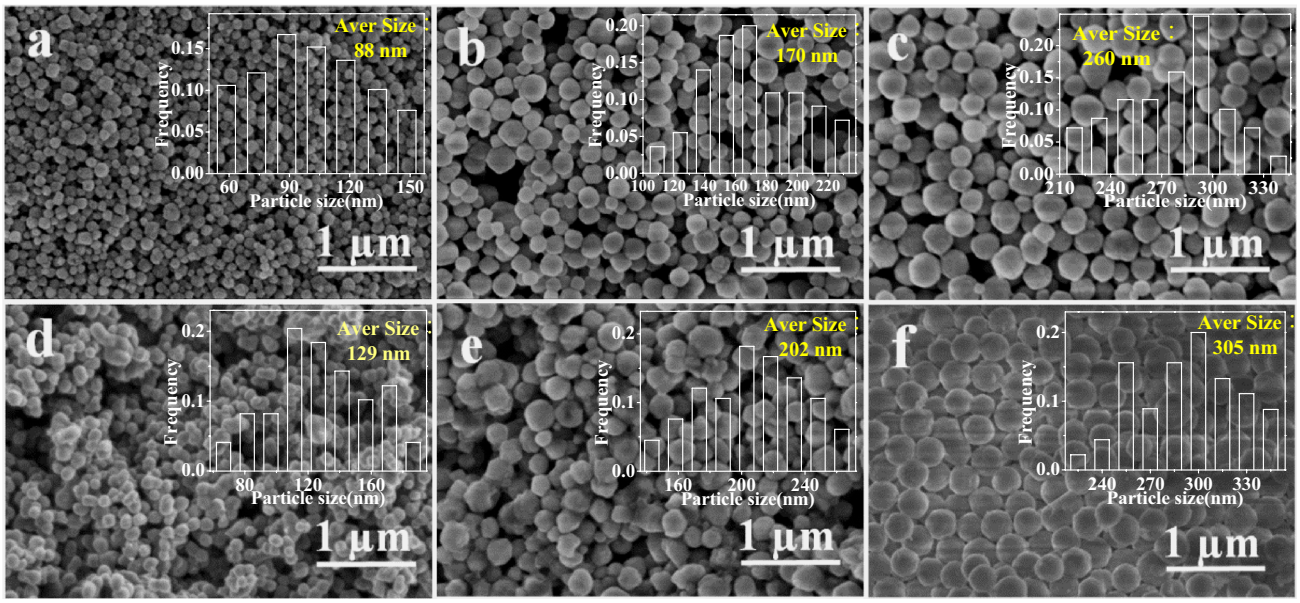

Fig. 7 SEM images of C-BTO$_x$ and C-BTO$_x$@PR powders with different particle sizes (x = 1, 2, 3). **a** C-BTO$_1$ with a mean size of 88 nm, **b** C-BTO$_2$ with a mean size of 170 nm, **c** C-BTO$_3$ with a mean size of 260 nm, **d** C-BTO$_1$@PR with a mean size of 129 nm, **e** C-BTO$_2$@PR with a mean size of 202 nm, **f** C-BTO$_3$@PR with a mean size of 305 nm (The coating content of PR is 20 wt%.)

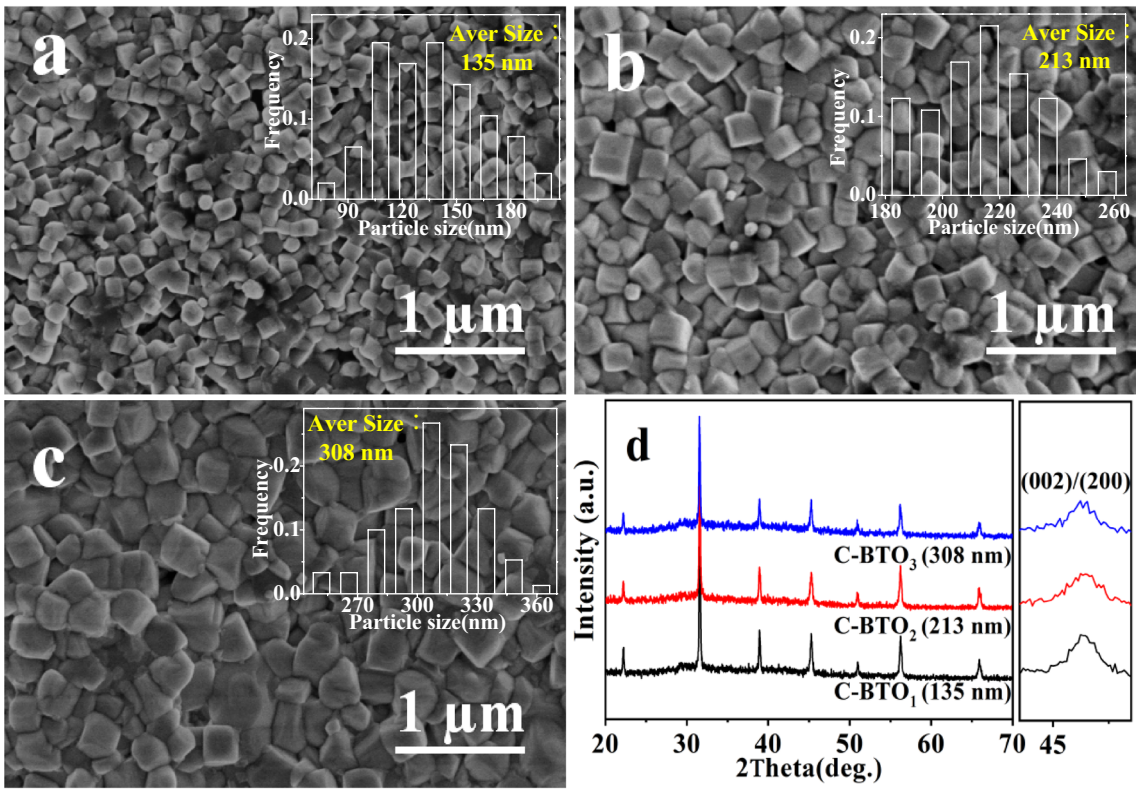

Fig. 8 SEM images and XRD patterns of C-BTO$_x$ ceramics (x = 1, 2, 3). **a** C-BTO$_1$ with a mean size of 135 nm, **b** C-BTO$_2$ with a mean size of 213 nm, **c** C-BTO$_3$ with a mean size of 308 nm, **d** XRD patterns

powders. Since smaller powders have more surface energy and defect energy, the larger sintering activity tend to lower their sintering activation energy and the optimal T_s [18]. In a certain sample, PR has two positive effects. One is to prevent the agglomeration of $BaTiO_3$, the other is that it acts as an inhibitor of surface-surface transport to prevent the growth of grains in the early stage of sintering because the PR slowly decomposes, carbonizes and oxidizes, and it is conducive to the later densification. By the way, the agglomeration and uneven distribution during granulation will lead to abnormal growth of ceramic grains. Therefore, the PR coating will keep the size of the ceramic grains comparable to the powder particles, so as to achieve the purpose of controlling the grain size and lay the foundation for the preparation of micro-nanoceramic materials. Figure 8d is the XRD patterns of corresponding samples, which shows that all samples exhibit a perovskite structure without any impurity phase, and the c/a values are 0.9998, 1.0075 and 1.0082, respectively, as x = 1, 2, 3. The gradually increasing c/a value indicates the enhanced tetragonal phase from C-BTO$_1$ to C-BTO$_3$, which was caused by the gradual growth of ceramic grains as observed in Fig. 8a-c. More specifically, due to the split of the 002/200 peak at 45°, C-BTO$_3$ is a tetragonal phase (T phase), but the paraelectric cubic phase (C phase) is more stable in samples without this phenomenon including C-BTO$_1$ and C-BTO$_2$. Therefore, the C-BTO$_2$ size of 213 nm at the T-O phase transition here could be considered as the threshold value of the particle size of nanoceramics. It is generally acknowledged that in normal ferroelectrics, ferroelectric domains are formed to alleviate the grain boundary stress caused by the increase of the unit cell volume. However, in BT ceramics with smaller grain sizes, the internal stress at the grain boundaries cannot be eliminated by the formation of domains, so the weaker ferroelectricity makes the paraelectric cubic phase more stable in C-BTO$_1$ sample.

Figure 9 shows the temperature dependence of dielectric permittivity and dielectric loss of C-BTO$_x$ ceramics after coated with PR, and their parameters are tabulated in Table 1. From the test results, the ε_{max} of the sintered C-BTO$_1$, C-BTO$_2$ and C-BTO$_3$ ceramics is 2012, 2533 and 3037. The corresponding T_c (the responding temperature of the ε_{max}) is 103.9 °C and 116.0 °C of C-BTO$_2$ and C-BTO$_3$, respectively, while no obvious peak of dielectric constant named Curie temperature can be observed. Owing to the consistently pretty density in all samples, the electrical performance of ceramics depends highly on their particle size change and the corresponding phase structure there. It can be confirmed that over the whole temperature range, as the grain size increases, the

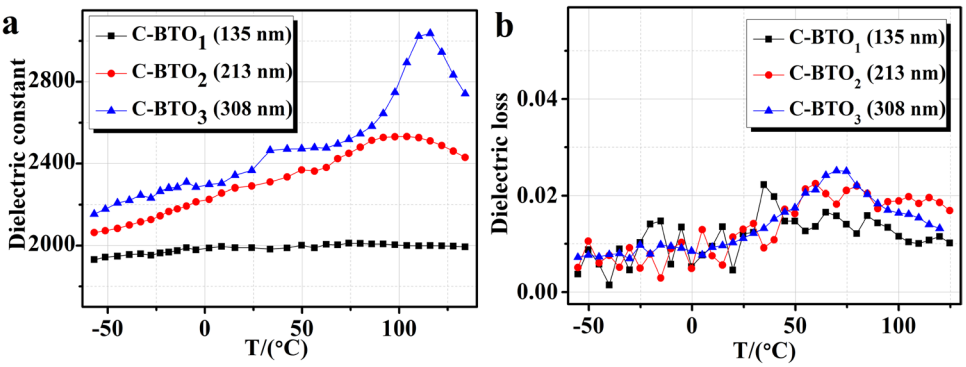

Fig. 9 Temperature dependence of **a** dielectric permittivity and **b** dielectric loss of C-BTO$_x$ ceramics ($x = 1, 2, 3$)

Table 1 Parameters about the structure and performance of the C-BTO$_x$ nanoceramics ($x = 1, 2, 3$)

Specimens	C-BTO$_1$	C-BTO$_2$	C-BTO$_3$
Sintering condition	940 °C 2 h	980 °C 2 h	1060 °C 2 h
a (Å)	3.9981	3.9975	3.9956
c (Å)	3.9973	4.0275	4.0284
c/a	0.9998	1.0075	1.0082
Relative density (%)	97.3%	98.8%	96.9%
Grain size (nm)	135 ± 22	213 ± 15	308 ± 10
T_c (°C)	/	103.9	116.0
ε_{max}	2012	2533	3037
Tanδ (25 °C)	0.0120	0.0130	0.0111

values of the dielectric constant obviously elevate and T_c shifts toward higher temperature. The grain size effect upon the dielectric properties of $BaTiO_3$ ceramics may be attributed to two major models including the intrinsic internal stress model and the extrinsic "dead layer" model [5]. The intrinsic internal stress model refers to that as the particle size increases, the increased number of 90 °C domains can fully offset the internal stress during the phase transition. So, the easier phase transition tends to increase the content of the tetragonal phase. Except for it, the extrinsic "dead layer" model is another factor. The volume fraction of grain boundary in non-ferroelectric phase increases as the decrease of grain size, thus lowering the proportion of ferroelectricity in smaller-sized ceramics. Combining all above, with the decrease of grain size, the proportion of the Curie temperature and ferroelectricity decreases, resulting in more diffused phase transition. Analogous phenomenon has also been observed in the submicron $BaTiO_3$ ceramics [40]. Meanwhile, the dielectric peaks near phase transition become more broader and diffuse with decreasing the grain size, so the relative flat dielectric temperature curve in sample with smaller size means their good temperature coefficient of capacitance. Besides, the loss values are all within a lower range, which are mainly attributed to their optimal microscopic compactness.

4 Conclusions

In this paper, PR dispersant is used instead of PVA, and the core–shell structure of C-BTO@PR powder is constructed to prepare dense $BaTiO_3$ nanoceramics at a lower temperature. PR dispersant optimizes the dispersion of nanopowders in the granulation, and act as a grain growth inhibitor during sintering for nanoceramics. Results show that when the amount of PR is 0, 10, 20, 30 and 40 wt%, the coating thickness is 0, 8, 20, 28 and 37 nm, respectively. As the amount of PR coating increases, the ε_{max} and ε_r of $BaTiO_3$ ceramics first increase and then decrease, reaching their highest value at 20 wt% with relatively high ε_{max} of 3545 and low tanδ of 0.011. Furthermore, dense $BaTiO_3$ nanoceramics (135–308 nm) whose grain size comparable with the initial particle size can be controllably realized. Coating with PR in a core–shell manner is an effective way to prepare dense nanoceramics.

Acknowledgements We thank the National Natural Science Foundation of China (Grant No. 21071115), the Shaanxi Province Natural Science Foundation Research Project (Grant No. 2020JZ-44), and the Key Science and Technology Innovation Team of Shaanxi Province (2019TD-007) for funding our research.

Compliance with ethical standards

Conflict of interest The authors declare that there is no conflict of interest.

References

1. Su XF, Riggs BC, Tomozawa M, Nelson JK, Chrisey DB (2014) Preparation of $BaTiO_3$/low melting glass core–shell nanoparticles for energy storage capacitor applications. J Mater Chem A 2(42):18087–18096

2. Zhong WL, Jiang B, Zhang PL, Ma JM, Cheng HM, Yang ZH, Li LX (1993) Phase transition in $PbTiO_3$ ultrafine particles of different sizes. J Phys Condens Matter 5:2619
3. Jiang B, Bursill LA (1999) Phenomenological theory of size effects in ultrafine ferroelectric particles of lead titanate. Phys Rev B 60:9978
4. Huang H, Sun CQ, Hing P (2000) Surface bond contraction and its effect on the nanometric sized lead zirconate titanate. J Phys Condens Matter 12:L127
5. Zhao Z, Buscaglia V, Viviani M, Buscaglia MT, Mitoseriu L, Testino A, Nygren M, Johnsson M, Nanni P (2004) Grain-size effects on the ferroelectric behavior of dense nanocrystalline $BaTiO_3$ ceramics. Phys Rev B 70:024107
6. Tian ZB, Wang XH, Zhang YC, Fang J, Song TH, Hur KH, Lee S, Li L (2010) Formation of core-shell structure in ultrafine-grained $BaTiO_3$-based ceramics through nanodopant method. J Am Ceram Soc 93(1):171–175
7. Jiang BB, Iocozzia J, Zhao L, Zhang HF, Harn YW, Chen YH, Lin ZQ (2019) Barium titanate at the nanoscale: controlled synthesis and dielectric and ferroelectric properties. Chem Soc Rev 48(4):1194–1228
8. Tian ZB, Wang XH, Shu L, Wang T, Song TH, Gui ZL, Li LT (2009) Preparation of nano $BaTiO_3$-based ceramics for multilayer ceramic capacitor application by chemical coating method. J Am Ceram Soc 92(4):830–833
9. Zhang YC, Wang XH, Kim JY, Tian ZB, Fang J, Hur KH, Li LT (2012) High performance $BaTiO_3$-based BME-MLCC nanopowder prepared by aqueous chemical coating method. J Am Ceram Soc 95(5):1628–1633
10. Makena IM, Shongwe MB, Machaka R, Masete MS (2020) Effect of spark plasma sintering temperature on the pore characteristics, porosity and compression strength of porous titanium foams. SN Appl Sci 2(4):1–8
11. Oghbaei M, Mirzaee O (2010) Microwave versus conventional sintering: A review of fundamentals, advantages and applications. J Alloy Compd 494(1–2):175–189
12. Heidary DSB, Lanagan M, Randall CA (2018) Contrasting energy efficiency in various ceramic sintering processes. J Eur Ceram Soc 38(4):1018–1029
13. Sun C, Wang X, Li L (2012) Low sintering of X7R ceramics based on barium titanate with SiO_2–B_2O_3–Li_2O sintering additives in reducing atmosphere. Ceram Int 38:S49–S52
14. Nakaiso T, Kageyama K, Ando A, Sakabe Y (2005) Preparation and characterization of $BaTiO_3$ thick films with Li_2O-SiO_2 sintering aid. Jpn J Appl Phys 44:6878–6880
15. Khalf AZ, Hall DA (2018) Influence of barium borosilicate glass on microstructure and dielectric properties of (Ba, Ca)(Zr, Ti)O_3 ceramics. J Eur Ceram Soc 38(13):4422–4432
16. Shi Z, Guo ZX (2004) Kinetic modelling of binder removal in powder-based compacts. Mater Sci Eng A 365(1–2):129–135
17. Zemlyanoi KG (2013) Temporary technological dispersants in industry. Refract Ind Ceram 53:283–288
18. Gong HL, Wang XH, Zhang SP, Wen H, Li LT (2014) Grain size effect on electrical and reliability characteristics of modified fine-grained $BaTiO_3$ ceramics for MLCCs. J Eur Ceram Soc 34:1733–1739
19. Chen W, Zhao X, Sun JG, Zhang LX, Zhong LS (2016) Effect of the Mn doping concentration on the dielectric and ferroelectric properties of different-routes-fabricated $BaTiO_3$-based ceramics. J Alloy Compd 670:48–54
20. Yi Y, Lu Y, Wang J, Bai X, Pan Y, Yu Y, He C, Liu Y, Chen Y (2020) Structure and electrical properties of lead-free (1–x)$(K_{0.45}Na_{0.5}Li_{0.05})Nb_{0.95}Sb_{0.05}O_3$–x$(Ca_{0.95}Ba_{0.05})(Zr_{0.9}Sn_{0.1})O_3$ ceramics. SN Appl Sci 2:1–11
21. Kholodkova AA, Danchevskaya MN, Ivakin YD, Muravieva GP, Smirnov AD, Tarasovskii VP, Ponomarev SG, Fionov AS, Kolesovc VV (2018) Properties of barium titanate ceramics based on powder synthesized in supercritical water. Ceram Int 44:13129–13138
22. Bougoin M, Thevenot F (1987) Pressureless sintering of boron carbide with an addition of polycarbosilane. J Mater Sci 22(1):109–114
23. Schwetz KA, Grellner W (1981) The influence of carbon on the microstructure and mechanical properties of sintered boron carbide. J Less Common Met 82:37–47
24. Zhang H, Yan YJ, Huang ZR, Liu XJ, Jiang DL (2009) Pressureless sintering of ZrB_2-SiC ceramics: the effect of B_4C content. Scripta Mater 60(7):559–562
25. Li L, Liu C, Zhang LY, Wang TT, Yu H, Wang CG, Su ZM (2013) Multifunctional magnetic–fluorescent eccentric-(concentric-Fe_3O_4@SiO_2)@polyacrylic acid core–shell nanocomposites for cell imaging and pH-responsive drug delivery. Nanoscale 5(6):2249–2253
26. Su XF, Riggs BC, Tomozawa M, Nelson JK, Chrisey DB (2014) Preparation of $BaTiO_3$/low melting glass core-shell nanoparticles for energy storage capacitor applications. J Mater Chem A 2(42):18087–18096
27. Liu Y, Cui B, Wang Y, Ma R, Shangguan M, Zhao X, Wang S, Li Q, Wang Y (2016) Core-shell structure and dielectric properties of $Ba_{0.991}Bi_{0.006}TiO_3$@$Nb_2O_5$–$Co_3O_4$ ceramics. J Am Ceram Soc 99(5):1664–1670
28. Shangguan MQ, Cui B, Ma R, Wang YY (2016) Production of $Ba_{0.991}Bi_{0.006}TiO_3$@ZnO–$B_2O_3$–$SiO_2$ ceramics with a high dielectric constant, a core-shell structure, and a fine-grained microstructure by means of a sol-precipitation method. Ceram Int 42(6):7397–7405
29. Wang Y, Miao K, Ma R (2016) The formation of Y5V-type fine-grained ceramics based on spherical submicron $BaZr_{0.1}Ti_{0.9}O_3$@Al_2O_3 particles. Ceram Int 42(13):14627–14634
30. Du YC, Liu WW, Qiang R, Wang Y, Han XJ, Ma J, Xu P (2014) Shell thickness-dependent microwave absorption of core-shell Fe_3O_4@C composites. Acs Appl Mater Inter 6(15):12997
31. Rastegar H, Bavand-vandchali M, Nemati A, Golestani-Fardc F (2019) Phase and microstructural evolution of low carbon MgO-C refractories with addition of Fe-catalyzed phenolic resin. Ceram Int 45(3):3390–3406
32. Jin JH, Yang SC, Bae BS (2011) Network structure–property relationship in UV-cured organic/inorganic hybrid nanocomposites. Polym Chem 2(1):168–174
33. Chiang CL, Ma CCM (2004) Pressureless sintering of boron carbide with an addition of polycarbosilane. Polym Degrad Stabil 83:207–214
34. Yu D, Xu NX, Hu L, Zhang QL, Yang H (2015) Nanocomposites with $BaTiO_3$-$SrTiO_3$ hybrid fillers exhibiting enhanced dielectric behaviours and energy-storage densities. J Mater Chem C 3(16):4016–4022
35. Miyaura A, Kawaguchi T, Hagiwara M, Fujihara S (2019) Controlled 90° domain wall motion in $BaTiO_3$ piezoelectric ceramics modified with acceptor ions localized near grain boundaries. SN Appl Sci 1(4):286
36. Trick KA, Saliba TE (1995) Mechanisms of the pyrolysis of phenolic resin in a carbon/phenolic composite. Carbon 33:1509–1515
37. Dai B, Zheng P, Bai WF, Li L, Wu W, Ying Z, Zheng L (2018) Direct and converse piezoelectric grain-size effects in $BaTiO_3$ ceramics with different Ba/Ti ratios. J Eur Ceram Soc 38(12):4212–4219
38. Lee SK, Park TJ, Choi GJ, Koo KK, Kim SW (2003) Effects of KOH/BaTi and Ba/Ti ratios on synthesis of $BaTiO_3$ powder by coprecipitation/hydrothermal reaction. Mater Chem Phys 82(3):742–749
39. Ferkel H, Hellmig RJ (1999) Effect of nanopowder deagglomeration on the densities of nanocrystalline ceramic green bodies and their sintering behaviour. Nanostruct Mater 11(5):617–622

40. Zhao X, Hu Z, Yan Q, Wu T, Zhao L, Wang Y (2014) Fabrication of submicron La_2O_3-coated $BaTiO_3$ particles and fine-grained ceramics with temperature-stable dielectric properties. Scripta Mater 90:49–52